RSC Advances

ROYAL SOCIETY OF CHEMISTRY

www.rsc.org/advances

RSC Advances

ARTICLE

Highly sensitive and stabilized sensing 6-benzylaminopurine based on $NiCo_2O_4$ nanosuperstructures

Cite this: DOI: 10.1039/x0xx00000x

Received 00th January 2012,
Accepted 00th January 2012

DOI: 10.1039/x0xx00000x

www.rsc.org/

Lingshan Gong[a#], Huixiang Yan[a#], Hong Dai[a*], Shupei Zhang[a], Yilin Li[a], Qingrong Zhang[a], Yanyu Lin[b], Zhensheng Hong[a**]

$NiCo_2O_4$ nanosuperstructures which were synthetized by facile hydrothermal method were developed for the determination of 6-benzylaminopurine (6-BAP). As a new-style electric material, $NiCo_2O_4$ can be utilized to structure an ultrasensitive and prominent stable electrochemical sensor. The electrochemical investigation confirmed that $NiCo_2O_4$ nanosuperstructures stabilized via polyethyleneimine (PEI) could remarkably boost the electrocatalytic activity for the oxidation response of 6-BAP owing to its unique properties of large pore volume, good electrical conductivity and metal catalysis. The detailed electrochemical behavior of 6-BAP at PEI-$NiCo_2O_4$/GCE exhibited the higher peak current and more negative oxidation potential than bare glassy carbon electrode (GCE), simultaneously its kinetic and thermodynamic parameters were further calculated, indicating that this sensing platform accomplished excellent electrochemical catalysis towards 6-BAP. The fabricated sensor of PEI-$NiCo_2O_4$/GCE for 6-BAP presented a wide linear range from 10^{-10} to 10^{-5} M with a low detection limit of 0.1 nM. The modified electrode exhibited long-term stability and high sensitivity was shown fine practicability in food born contamination and even broader applications.

Introduction

6-benzylaminopurine (6-BAP) is a class of chronic toxic substances, getting extra doses of it could cause mucous membranes, upper respiratory tract, eyes, skin irritation and even cancer [1]. Therefore, it was necessary to develop an effective and ultrasensitive approach to determine 6-BAP. Up to now, many methods were developed to determine 6-BAP，such as ultraviolet-visible spectroscopy (UV-vis) photometry [2], high performance liquid chromatography (HPLC) [3], and electrochemical methods [4, 5]. However, the sensitivity of UV-vis was limited, and not suitable for trace level of 6-BAP. HPLC, its mobile phases almost were poisonous and in large amount of consumption when assaying. Thus, electrochemical method was a better choice for 6-BAP analysis, because it performed many remarkable advantages, especially speediness, cost saving, achieving real-time detection [4]. To improve the stability and sensitivity of 6-BAP determination, various modified materials were used for constructing ultrasensitive electrochemical sensors. Porous materials were received considerable attention because of their high porosity and large surface area.

Recently, the spinel nickel cobaltite ($NiCo_2O_4$) was one kind of highly conductive binary metal oxides, dramatically regarded as a desirable electrode material due to its inherent conductivity characteristic [6]. Typically, the nanosuperstructure [7] of $NiCo_2O_4$ was composed of uniform small granules, resulting in increasing the specific area and offering an open three-dimensional (3D) structure to accommodate a large amount of superficial electroactive species for participation during the electrochemical reaction [8, 9]. Nevertheless, there was hardly paper reporting the research about the electrocatalytic activity of $NiCo_2O_4$ stabilized by polyethyleneimine (PEI) to apply for analysis practical samples.

The nanosuperstructure of $NiCo_2O_4$ was tightly anchored to the surface of electrode by PEI, with merit of good conductivity and large surface area, which could strongly improve the performances of fast electron transport pathways and electrochemical activity [8]. So the PEI-$NiCo_2O_4$ modified film was an excellent electro-oxidation catalyst sensor for the highly sensitive determination of 6-BAP. Consequently, this electrochemical sensor showed good performances, such as easy constructive process, low cost, stable, rapid, sensitive response as well as wide linear range. Furthermore, this PEI-$NiCo_2O_4$ modifier was prospective to develop a new-type chemical sensor applying for other food borne contamination with high sensitivity and stability.

Experimental

Synthesis of $NiCo_2O_4$ nanosheets

Preparation of the porous $NiCo_2O_4$ nanosuperstructure was synthesized as follows: 4.5 mM of hexamethylenetetramine, 2 mM of $Co(NO_3)_2 \cdot 6H_2O$ and 1 mM of $Ni(NO_3)_2 \cdot 6H_2O$ were dissolved in the solution, containing 40 mL deionized water and 20 mL ethanol. Then the mixture solution was transferred into 100 mL Teflon-lined stainless steel autoclave and maintained at 150 ºC for 12 h. When cooling to room temperature, the precipitates were collected by centrifugation, washed with ethanol and water repetitiously. The production need to dry in the blast oven at 60 ºC overnight. Finally, the product was annealed at 350 ºC for 2 h in air in order to obtain porous $NiCo_2O_4$ nanosheets.

Preparation of modified electrodes

A bare glass carbon electrode (GCE, 3 mm in diameter) was obtained by burnished on chamois with 0.3 μm alumina particles, then washed with ethanol and water repetitiously and natural dried in air on standby before use. It was dripped down 3 μL 0.2 mg mL^{-1} PEI on the prepared bare GCE, air-dried and then obtained PEI/GCE. Additionally, for preparation of PEI-$NiCo_2O_4$ modified electrode (PEI-$NiCo_2O_4$/GCE), 0.2 mg mL^{-1} PEI was added into 3 mg mL^{-1} $NiCo_2O_4$ solution. With a microinjector, 3 μL of PEI-$NiCo_2O_4$ solution was deposited on the freshly prepared GCE surface, and displaced below infrared lamp to dry, when it cooled to room temperature then gained PEI- $NiCo_2O_4$/GCE.

Results and discussion

Characterization of $NiCo_2O_4$

The morphological analysis of the spinel $NiCo_2O_4$ nanosuperstructures was shown by scanning electron microscopy (SEM) image in Fig. 1A. Obviously, the resulting product was composed of nanosheets like leaves morphologies with lots of serration increasing interconnected sites to form a typical three-dimensional structure. Especially, these nanosheets also exhibited lots of open space and electroactive surface sites between them, which could enhance the contact area with electrolyte and fast electron transport process. Transmission electron microscopy (TEM) was further carried out to investigate the structure of the $NiCo_2O_4$ nanosheets shown in Fig. 1B. It indicated this nanosuperstructures may be constructed with the granules at approximate 10-15 nm diameter, and the bright area seems like some mesopores [10], providing tremendous active sites for electro-catalysis during the redox reaction. To further understand the composition and structure of the $NiCo_2O_4$ samples, the phases of the $NiCo_2O_4$ were indentified by X-ray diffraction (XRD) showing in Fig. 1D, and the typical XRD patterns were assigned to (111), (220), (311), (222), (400), (422), (511), and (440) plane reflections of the spinel $NiCo_2O_4$ crystalline structure, which were consistent with the standard JCPDS (card no. 73-1702), suggesting that this $NiCo_2O_4$ was the formation

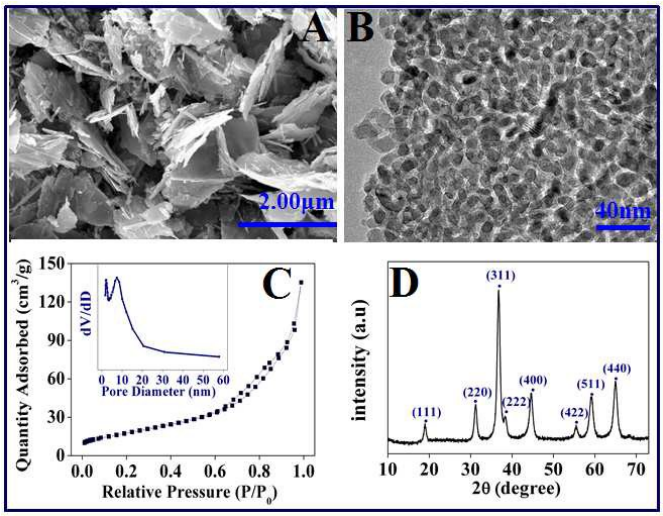

Fig. 1 (A) SEM image of $NiCo_2O_4$. (B) TEM image of $NiCo_2O_4$. (C) N_2 adsorption-desorption isotherm of $NiCo_2O_4$. Inset shows the corresponding BJH pore size distribution of $NiCo_2O_4$. (D) XRD pattern of $NiCo_2O_4$.

of homogeneous spinel phase with different exposed crystal planes [11]. The porous characteristics of $NiCo_2O_4$ were also investigated by nitrogen adsorption-desorption isotherm measurement shown in Fig. 1C. It was seen that the typical hysteresis loop in the relative pressure rang of 0.6-1.0 P/P_0 and demonstrated the presence of mesopores [12]. As shown in the inset of Fig. 1C, from the Barret-Joyner-Halenda (BJH) pore size distribution curve, it could be observed the wide ranging distribution of mesopores [13]. Therefore, it could be concluded that the $NiCo_2O_4$ nanosuperstructures exhibited large pore volume, abundant open space and electroactive surface sites [14], which could contribute to the activity, selectivity and stability of the electrode.

Electrochemical characterization of GCE, PEI/GCE, PEI-$NiCo_2O_4$/GCE

Under the optimal conditions (Fig. S1), the electrochemical characterization of different modified electrodes was investigated by cyclic voltammetry (CV) in 5mM potassium hexacyanoferrate containing 0.1 M potassium chloride as it was shown in Fig. 2A. Both the modified and unmodified electrodes have the good reversibility towards $K_3[Fe(CN)_6]$ solution. And the redox peak current of PEI-$NiCo_2O_4$/GCE (curve c) was highest than those of GCE (curve a) and PEI/GCE (curve b), revealing the best conductive and particular catalytic activity of PEI-$NiCo_2O_4$/GCE among the other electrodes. Moreover, owing to PEI contained highly positive charge [15], when $NiCo_2O_4$ added to PEI solution as the modified film, the synergistic effects formed at the modified layer, which might be caused by the fact that $NiCo_2O_4$ was a mesoporous material with large surface area, good electrochemical activity, and the possibility of promoting electron transfer reactions at a lower overpotential [11]. There was the peak current of PEI increased

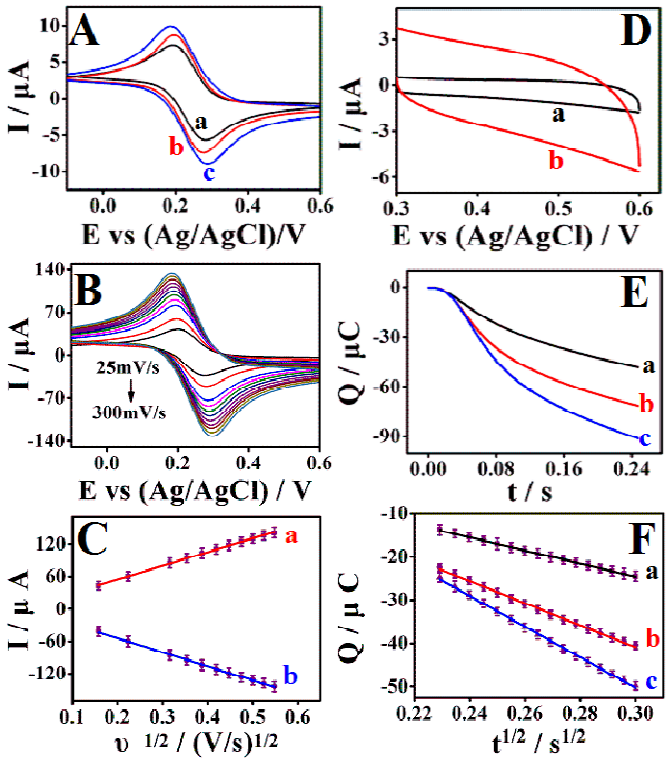

Fig. 2 (A) Cyclic voltammograms of bare GCE(a), PEI/GCE(b), PEI-$NiCo_2O_4$/GCE(c) in 5 mM $K_3[Fe(CN)_6]$ and 0.1M KCl containing 0.1 M PBS (pH 7.0) at 100 mV s^{-1} scan rate. (B) Cyclic voltammograms of PEI-$NiCo_2O_4$/GCE in 5 mM $K_3[Fe(CN)_6]$ containing 0.1 M KCl at various scan rates from 25 mV s^{-1} to 300 mV s^{-1}. (C) The linear relationship between the peak currents (line a is the anode peak current, line b is the cathode peak current) and the square root of the scan rates. (D) Cyclic voltammograms of bare GCE (a, black line) and PEI-$NiCo_2O_4$/GCE (b, red line) in 1.0 M KCl solution range from 0.3 V to 0.6 V versus Ag/AgCl as reference electrode at 100 mV s^{-1} scan rate. (E) Chronocoulometry of bare GCE(a), PEI/GCE(b), PEI-$NiCo_2O_4$/GCE(c) in 5 mM $K_3[Fe(CN)_6]$ and 0.1 M KCl containing 0.1 M PBS (pH 7.0). (F) The linear relationship between the charge and the square root of scan time on bare GCE(a), PEI/GCE(b), PEI-$NiCo_2O_4$/GCE(c)

with the scan rates from 25 mV s^{-1} to 300 mV s^{-1} shown in the Fig. 2B. As seen in the Fig. 2C, the relationship of the peak currents and the square of scan rates was in great linearity, indicating this electrochemical reaction process on the PEI-$NiCo_2O_4$/GCE sensing interface was a diffusion control process. In order to investigate the electrochemical surface active area, it could be seen that chronocoulometry of $K_3[Fe(CN)_6]$ respectively at the GCE (curve a), PEI/GCE (curve b) and PEI-$NiCo_2O_4$/GCE (curve c) shown in the Fig. 2E. Based on the slope of relationship of Q and $t^{1/2}$ shown in the Fig. 2F, the electrode active area could be calculated according to the following equation [16]:

$$Q(t) = \frac{2nFAcD^{1/2}t^{1/2}}{\pi^{1/2}} + Q_{ads} \quad (1)$$

Herein, n is the number of transferred electron, D is the diffusion coefficient of $K_3[Fe(CN)_6]$, Q_{ads} is Faradic charge, c is the concentration of $K_3[Fe(CN)_6]$, F and π have usual values. By calculating, the value of the electrode active areas of GCE was 0.071 cm^2, PEI/GCE was 0.111 cm^2 and PEI-$NiCo_2O_4$/GCE was 0.152 cm^2, suggesting the PEI-$NiCo_2O_4$/GCE had the largest electroactive surface area comparing with the bare GCE and PEI/GCE. Furthermore, the capacitance ability of modified layer was investigated by CV shown in Fig. 2D and its value could be calculated following the equation [17]: C_{CV}= i / (sυ), where i, s, υ respectively are average charge or discharge current (A), surface area (cm^2) and scan rate (V s^{-1}). So the capacitance of GCE (curve a) and PEI-$NiCo_2O_4$/GCE (curve b) respectively calculated to be 107.4 μF cm^{-2} and 352.9 μF cm^{-2}, that was to say the capacitance of PEI-$NiCo_2O_4$/GCE was 3 times higher than GCE, so this sensor of PEI-$NiCo_2O_4$/GCE had an excelled capacitance electrode performance. Moreover, the leaves-like $NiCo_2O_4$ nanosheets with different exposed crystal planes exhibited prominent electrochemical catalysis [18], because PEI-$NiCo_2O_4$ had the feasibility of a conduction pathway of electrons from the analyte and the electrode.

Electrocatalytic activity of PEI-$NiCo_2O_4$/GCE towards 6-BAP

To the best of our knowledge, the current density was an important value for aiming qualitative information about the electrochemical reactions [19]. And according to the equation: J = I / S, where J is the current density, I is the current, S is the surface area of electrode. The electrochemical characterization of different modified electrodes towards 6-BAP was investigated by current density shown in Fig. 3A. A weak oxidation peak was observed at bare GCE with potential about 1.01 V (curve a). In contrast, it was clear that the peak current density recorded at PEI/GCE (curve b) was higher than the bare GCE, and the oxidation peak potential was about 0.99 V, which was less positive than the bare GCE. PEI-$NiCo_2O_4$/GCE performed the highest oxidation peak, the peak current density was 6.5 A m^{-2} and the most negative potential about 0.93 V than other electrodes, owing to spinel $NiCo_2O_4$ nanosheets possessed good electrical conductivity and high electrochemical activity[16,20]. Based on these advantages of PEI-$NiCo_2O_4$/GCE, it was expected to provide an excellent analytical performance, sensitivity, and detectability towards 6-BAP.

For further investigate the reaction characters of 6-BAP at PEI-$NiCo_2O_4$/GCE, the effect of scan rates (υ) on the electrochemical behavior of 6-BAP was validated by linear sweep voltammogram (LSV) shown in Fig. 3B. It was found that peak potential (E_{pa}) shifts positively accompanied with the increase of peak current (I_{pa}) upon the increase of scan rates. As shown in Fig. 3C, the linear relationship of E_{pa} and natural logarithm of scan rates was cited as the calibration equation of E_{pa} (V) = 0.0242 ln υ +1.5756 (R^2 = 0.9987), which followed the equation [21]:

$$E_{pa} = E^0 + \frac{RT}{\alpha nF}\ln\frac{RTK^0}{\alpha nF} + \frac{RT}{\alpha nF}\ln\upsilon \quad (2)$$

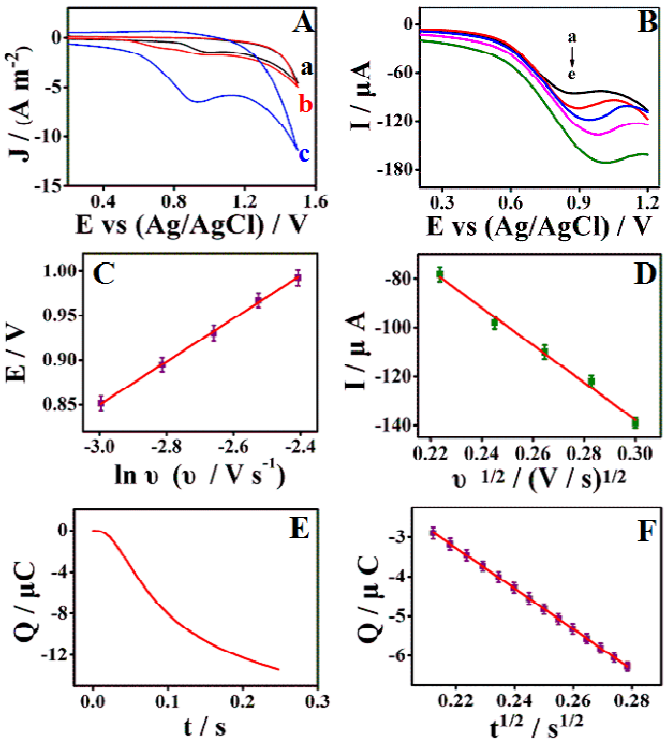

Fig. 3 (A) Current density of bare GCE (a), PEI/GCE (b), PEI-$NiCo_2O_4$/GCE (c) at 100 mV s^{-1} scan rate. (B) LSVs of PEI-$NiCo_2O_4$/GCE at different scan rates. (C) The linear relationship of E-ln υ. (D) The linear relationship of I-υ $^{1/2}$. (E) Chronocoulometry of PEI-$NiCo_2O_4$/GCE. (F) The linear relationship of Q-$t^{1/2}$ in 0.1 mM 6-BAP containing 0.1 M PBS (pH 8.5).

Moreover, according to the Eq. (2), the value of α was 0.5 in the totally irreversible electrochemical reaction. Thus, the number of electron transferred (n) could be easy gained 2 by the slope of E-ln υ in the Fig. 3C. Based on the above results and earlier published report [22], a tentative overall 6-BAP oxidation reaction at PEI-$NiCo_2O_4$/GCE could be described as follows:

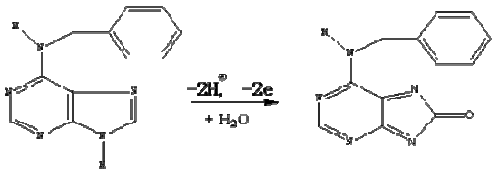

(3)

In addition, the good linear relationship of currents and the square root of scan rates (I-$υ^{1/2}$) was shown in the Fig. 3D, I_p = -24.135 $υ^{1/2}$ + 91.43, R^2 = 0.9903. It indicated the 6-BAP oxidation on PEI-$NiCo_2O_4$/GCE was a diffusion-controlled transfer process which involves two-electron and two-proton transfer (Fig. S2).

To obtain the value of the diffusion constant of 6-BAP, it was investigated that the chronocoulometry of 6-BAP had a good response based on the PEI-$NiCo_2O_4$/GCE shown in Fig. 3E, furthermore, the relationship of Q-$t^{1/2}$ from the Fig. 3F accorded to the Anson equation [16]:

$$Q(t) = \frac{2nFAcD^{1/2}t^{1/2}}{\pi^{1/2}} + Q_{ads} \quad (4)$$

In this system, the slope of Q-$t^{1/2}$ was 34 from the calibration equation as Q (μC) = -34.048 $t^{1/2}$ – 2.1258 (R^2 = 0.9985), n = 2, F = 96500, A = 0.152 cm^2, then $D_{6\text{-BAP}}$ = 1.08×10^{-4} cm^2 s^{-1} could be easy concluded. Meanwhile, the value of the standard heterogeneous rate constant (k_s) of the 6-BAP could be calculated from the following equation [23]:

$$k_s = 2.4\times\exp(-\frac{0.02F}{RT})\bullet D^{1/2}\bullet(E_p - E_{p/2})^{-1/2}\bullet v^{1/2} \quad (5)$$

Herein, the value of the $E_{p/2}$ was 0.72 V, when the current was half of the peak current. Thus, the k_s was 3.16×10^{-3} cm s^{-1} for 6-BAP which was larger than the literatures reported [5], suggesting the oxidation progress of 6-BAP on the PEI-$NiCo_2O_4$/GCE with a faster sensing rate, exhibiting highly electrocatalytic activity.

The apparent activation energy (E_a) of 6-BAP

The thermodynamic parameters of the apparent activation energy (E_a) was determined by examining the effect of temperature on LSV behavior of 6-BAP range from 0 V to 1.5 V versus Ag/AgCl as reference electrode at 100 mV s^{-1} scan rate. The linear relationship between the reciprocals temperature and the natural logarithm of peak current respectively on PEI/GCE (curve a) and PEI-$NiCo_2O_4$/GCE (curve b) was shown in the Fig. 4. The current intensity of peaks was increased with elevation of temperature, and the slope of curve (a) was larger than the curve (b) showing at the

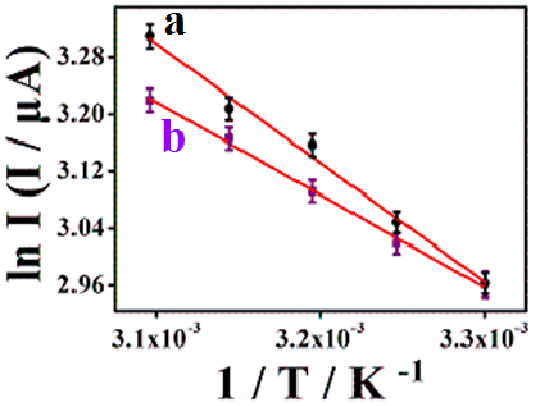

Fig. 4 The relationship of PEI/GCE (a) and PEI-$NiCo_2O_4$/GCE (b) between naturally logarithm of peak current and 1/T in 0.1 mM 6-BAP containing 0.1 M PBS (pH 8.5) range from 0 V to 1.5 V versus Ag/AgCl as reference electrode at 100 mV s^{-1} scan rate.

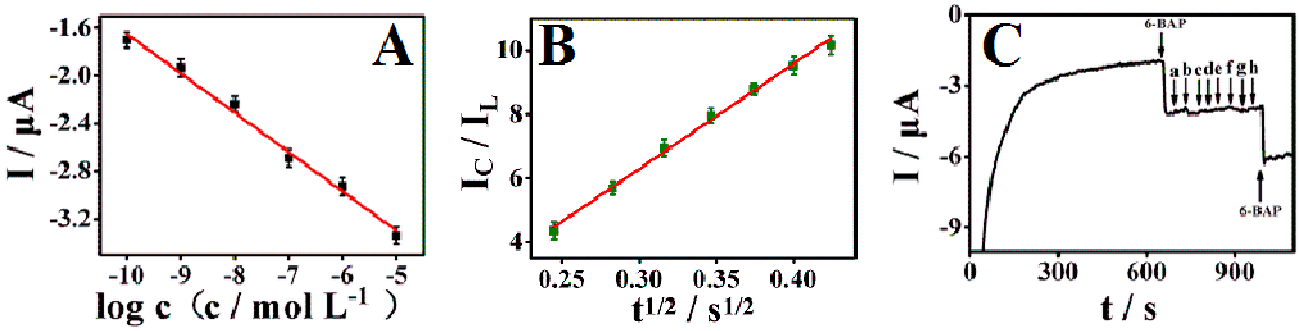

Fig. 5 (A) The plot of chronoamperometry current against the logarithm of 6-BAP concentrations at 0.93 V versus Ag/AgCl as reference electrode at 100 mV/s scan rate. (B) The linear relationship between I_C/I_L and $t^{1/2}$. (C) Interference test of PEI-$NiCo_2O_4$/GCE in 0.1 M PBS (pH 8.5) with 5×10^{-6} M 6-BAP in presence of 5×10^{-5} M VB_1 (a), VB_2 (b), AA (c), valine (d) and proline (e); 5×10^{-4} M Fe^{3+} (f), K^+ (g) and Zn^{2+} (h).

calibration equations: $I_{PEI/GCE}$ (μA) = -1296/T + 8.4 (R^2 = 0.9893) and $I_{PEI\text{-}NiCo2O4/GCE}$ (μA) = -973/T + 7.2 (R^2 = 0.9985), suggesting that the oxidation of 6-BAP on PEI/GCE need more energy than on the PEI-$NiCo_2O_4$/GCE. The values of E_a could be calculated by the following equation [24]:

$$\ln I = \frac{E_a}{RT} + \ln A \qquad (6)$$

Thus, the apparent activation energy of 6-BAP on PEI/GCE and PEI-$NiCo_2O_4$/GCE were respectively 10.77 and 8.09 kJ mol^{-1}. The lower energy of PEI-$NiCo_2O_4$/GCE revealed that the electrochemical of oxidation process of 6-BAP on PEI-$NiCo_2O_4$/GCE was easier to occur than on PEI/GCE [25]. It was suggested that PEI-$NiCo_2O_4$ had high electrochemical activity and good electron transferred ability, due to the characteristic of superior electronic conductivity and metal catalysis of $NiCo_2O_4$ nanosuperstructures.

The catalytic rate constant (k_h) by chronoamperometry investigations

It could be seen that the relationship between I_C/I_L and $t^{1/2}$ under the optimal potential of 0.93V was investigated in the Fig. 5B. Therefore, the catalytic rate constant for the oxidation of 6-BAP at PEI-$NiCo_2O_4$/GCE could be determined according to the equation [26]:

$$i_C / i_L = \gamma^{1/2}\left[\pi^{1/2} erf(\gamma^{1/2}) + \exp(-\gamma)/\gamma^{1/2}\right] \qquad (7)$$

Where I_C and I_L were the currents at PEI-$NiCo_2O_4$/GCE in presence and absence of 6-BAP, $\gamma = k_h c_0 t$ was the argument of error function, the other parameters had their usual meanings. In cases the error function was almost equal to 1 and therefore the above equation could be reduced to the following equation:

$$i_C / i_L = \pi^{1/2}\gamma^{1/2} = \pi^{1/2}(k_h c_0 t)^{1/2} \qquad (8)$$

Utilizing the slope of calibration equation as $I_C/I_L = 32.59\ t^{1/2} - 3.4924$ (R^2 = 0.9955) in the Fig. 5B, the k_h value was calculated to 3.38×10^6 cm^3 mol^{-1} s^{-1}, which indicated that the electro-oxidation of 6-BAP had a high catalytic rate on this modified electrode of PEI-$NiCo_2O_4$/GCE based on the PEI-$NiCo_2O_4$ material exhibition of good catalytic activity and inherent electrical conduction. Eventually, an expected conclusion could be drawn that the excellent electrocatalytic activity and high electrochemical performances towards 6-BAP were achieved at PEI-$NiCo_2O_4$/GCE.

Calibration curve

The relationship between I_{pa} and the logarithm of the concentration of 6-BAP was illustrated in the Fig. 5A. As seen, the peak current was proportional to the concentrations of 6-BAP in the range from 10^{-10} to 10^{-5} M, and the calibration equation was I_{pa} (μA) = 4.966 - 0.3324 log C (R^2 = 0.9905) with a low detection limit of 0.1 nM, which was lower than recent reports (shown in Table S1). This sensor of PEI-$NiCo_2O_4$/GCE platform possessed excellent high sensitivity towards the application.

Selectivity, reproducibility and stability

Selectivity of PEI-$NiCo_2O_4$/GCE for the determination of 6-BAP was investigated by chronoamperograms to evaluate the effects of the possible interferences in bean sprout samples. The 6-BAP is often with some electroactive biomolecules in fruits and vegetables, including inorganic metal ions and antioxidants such as vitamin B_1 (VB_1), vitamin B_2 (VB_2), ascorbic acid (AA), valine, proline, Fe^{3+}, Zn^{2+} and K^+. Hence, the selectivity of PEI-$NiCo_2O_4$/GCE was examined by monitoring the influence of these interfering molecules in presence of 5×10^{-6} M of 6-BAP shown in the Fig. 5C. As seen, even though 10-fold concentration of vitamin B_1, vitamin B_2, AA, valine, proline and 100-fold concentration of Fe^{3+}, Zn^{2+} and K^+ had no influence on the determination of 6-BAP, resulting that this constructed method was adequate for the determination of 6-BAP in practical samples (Table S2) with good selectivity which could be contributed to the further detect other contaminations.

The reproducibility and repeatability of PEI-$NiCo_2O_4$/GCE for the established current response in 0.1 mM 6-BAP was investigated showing in the Fig. S3. The peak current of 6-BAP was determined

by five PEI-$NiCo_2O_4$ modified electrodes with the same conditions at three days, showing that the relative standard deviation (RSD) was 4.6 %. This result suggested the high level of repeatability between different electrodes. In order to investigate the storage stability of the senor, the PEI-NiCo2O4/GCE was stored in PBS (pH 8.5) at 4 ºC in the refrigerator when not being in use. It was found that the current responses remained about 90 % of the initial values. Therefore, this sensor of PEI-$NiCo_2O_4$/GCE has good storage stability towards the application.

Conclusion

Herein, $NiCo_2O_4$ nanosuperstructures in a novel synthesis method were used as a fantastic electric material. The electrochemical sensor based on $NiCo_2O_4$ nanosuperstructures was in excellent electric activity, owing to the porous characteristics of $NiCo_2O_4$, resulting in great electrocatalytic activity towards the oxidation process of 6-BAP with a low detection limit of 0.1 nM. The fabricated PEI-$NiCo_2O_4$/GCE testified strong catalytic activity and excellent electrochemical stability by its systemic kinetic and thermodynamic parameters. The experiments results demonstrated that PEI-NiCo2O4/GCE electrochemical sensor extended a feasible approach to detect rudimental contaminations of vegetables and fruits with high sensitivity, stability, reproducibility and selectivity.

Acknowledgment

This project was financially supported by NSFC (21205016, 21575024, 51502038), National Science Foundation of Fujian Province (2011J05020), Education Department of Fujian Province (JA14071, JB14036, JA13068), Foundation of Fuzhou Science and Technology Bureau (2015-S-160).

Notes and references

[a] *College of Chemistry and Chemical Engineering, Fujian Normal University, Fuzhou 350108, P. R. China, Fax: (+86)-591-22866135,E-mail: dhong@fjnu.edu.cn*
[b] *Fujian Provincial Key Laboratory of Quantum Manipulation and New Energy Materials, College of Physics and Energy, Fujian Normal University, Fuzhou 350108, P. R. China. E-mail: winter0514@163.com*
[c] *Ministry of Education Key Laboratory of Analysis and Detection for Food Safety, and Department of Chemistry, Fuzhou University, Fuzhou 350002, P. R. China*
[#] *These authors contributed equally to this study.*

Fig. S Futhure analysis on Optimization of detection conditions; Table S1 Comparable figures of determining 6-benzylaminopurine; Table S2 The results of addition recovery test. See DOI: 10.1039/b000000x/

1 Y. F. Zhang, X. J. Bo and L. P. Guo, *Anal. Methods*, 2012, 4, 736.
2 G. Woldemichael, T. Tulu and G. U. Flechsig, *Microchim. Acta*, 2012, 179, 99.
3 S. Lee, G. Y. Kim and J. H. Moon, *Anal. Methods*, 2013, 5, 961.
4 G. Zhao, K. Z. Liu, S. Lin, J. Liang, X. Y. Guo and Z. J. Zhang, *Microchim. Acta*, 2003, 143, 255.
5 D. Sun, H. J. Zhang, *Anal. Chim. Acta*, 2006, 557, 64.
6 H. C. Chen, J. J. Jiang, L. Zhang, D. D. Xia, Y. D. Zhao, D. Q. Guo, T. Qi and H. Z. Wan, *J. Power Sources*, 2014, 248, 28.
7 T. J. Zhu, Q. S. Wu, P. Chen, Y. P. Ding, *J. Organomet. Chem.*, 2009, 694, 21.
8 T. Y. Wei, C. H. Chen, H. C. Chien, S. Y. Lu and C. C. Hu, *Adv. Mater.*, 2010, 22.
9 C. Yuan, J. Li, L. Hou, X. Zhang, L. Shen and X. W. Lou, *Adv. Funct. Mater.*, 2012, 22, 4592.
10 C. H. Wang, X. Zhang, D. C. Zhang, C. Yao and Y. W. Ma, *Electrochim. Acta*, 2012, 63, 220.
11 N. Padmanathan and S. Selladurai, *RSC Adv.*, 2014, 4, 8341.
12 H. Wang, J. L. Guo, C. Qing, D. M. Sun, B. X. Wang and Y. W. Tang, *Chem. Commun.*, 2014, 50, 8697.
13 M. U. A. Prathap and R. Srivastava, *Electrochim. Acta*, 2013, 108, 145.
14 Y. Li, L. L. Zou, J. Li, K. Guo, X. W. Dong, X. W. Li, X. Z. Xue, H. F. Zhang and H. Yang, *Electrochim. Acta*, 2014, 129, 14.
15 J. A. Syed, H. B. Lu, S. C. Tang and X. K. Meng, *Appl. Surf. Sci.*, 2015, 325, 160.
16 Y. H. Zhang, L. H. Wu, W. Lei, X. F. Xia, M. Z. Xia and Q. L. Hao, *Electrochim. Acta*, 2014, 146, 568.
17 L. H. Tang, Y. Wang, Y. M. Li, H. B. Feng, J. Lu and J. H. Li, *Adv. Funct. Mater.*, 2009, 19, 2782.
18 R. J. Zou, K. B. Xu, T. Wang, G. J. He, Q. Liu, X. J. Liu, Z. Y. Zhang and J. Q. Hu, *J. Materials Chemistry A*, 2013, 1, 8560.
19 B. Cheng, X. X. Zhang, *Electrochim. Acta*, 2014, 130, 785.
20 F. Wang, Y. J.Wu, K. Lu, L. Gao, B. X. Ye, *Electrochim. Acta*, 2014, 141, 82.
21 M. H. Pournaghi-Azar and R. Sabzi, *J. Electroanal. Chem.*, 2003, 543, 115.
22 S. S. Lu, Y. P. Wen, L. Bai, G. B. Liu, Y. X. Chen, H. Du and X. Q. Wang, *J. Electroanal. Chem.*, 2015, 750, 89.
23 J. Velasco, *Electroanalysis*, 1997, 9, 880.
24 R. B. H. Kacemm, N. Ouerfelli, J. V. Herraez, M. Guettari, H. Hamda and M. Dallel, *Fluid Phase Equilib.*, 2014, 383, 11.
25 Y. Wang, X. Wang, C. M. Li, *Appl. Catal. B: Environ.*, 2010, 99, 229.
26 J. H. Li, H. B. Feng, J. Li, Y. L. Feng, Y. Q. Zhang and J. B. Jiang, *Electrochim. Acta*, 2015, 167, 22

An ultrasensitive electrochemical sensor based on $NiCo_2O_4$ nanosuperstructures was proposed to determine 6-benzylaminopurine food borne contamination.